

# PARTICLE ACCELERATION, MAGNETIC FIELD GENERATION AND EMISSION FROM RELATIVISTIC JETS AND SUPERNOVA REMNANTS

K.-I. Nishikawa<sup>1</sup>, D. H. Hartmann<sup>2</sup>, P. Hardee<sup>3</sup>, C. Hededal<sup>4</sup>, Y. Mizunno<sup>5</sup>, and G. J. Fishman<sup>6</sup>

<sup>1</sup>*National Space Science and Technology Center, 320 Sparkman Drive, SD 50, Huntsville, AL 35805*

<sup>2</sup>*302C Kinard Laboratory Clemson University Clemson, SC 29634-0978*

<sup>3</sup>*Department of Physics and Astronomy, The University of Alabama, Tuscaloosa, AL 35487*

<sup>4</sup>*Dark Cosmology Center, Niels Bohr Institute, Juliane Maries Vej 30, , 2100 Copenhagen Ø, Denmark*

<sup>5</sup>*National Space Science and Technology Center, 320 Sparkman Drive, SD 50, Huntsville, AL 35805*

<sup>6</sup>*NASA-Marshall Space Flight Center, National Space Science and Technology Center, 320 Sparkman Drive, SD 50, Huntsville, AL 35805*

## ABSTRACT

We performed numerical simulations of particle acceleration, magnetic field generation, and emission from shocks in order to understand the observed emission from relativistic jets and supernova remnants. The investigation involves the study of collisionless shocks, where the Weibel instability is responsible for particle acceleration as well as magnetic field generation. A 3-D relativistic particle-in-cell (RPIC) code has been used to investigate the shock processes in electron-positron plasmas. The evolution of the Weibel instability and its associated magnetic field generation and particle acceleration are studied with two different jet velocities ( $\gamma = 2, 5$  - slow, fast) corresponding to either outflows in supernova remnants or relativistic jets, such as those found in AGNs and microquasars. Slow jets have intrinsically different structures in both the generated magnetic fields and the accelerated particle spectrum. In particular, the jet head has a very weak magnetic field and the ambient electrons are strongly accelerated and dragged by the jet particles. The simulation results exhibit jitter radiation from inhomogeneous magnetic fields, generated by the Weibel instability, which has different spectral properties than standard synchrotron emission in a homogeneous magnetic field.

Key words: particle acceleration, SNRs, simulations.

## 1. INTRODUCTION

Textbooks have long claimed that the shock conditions in supernova remnants provide the natural site for cosmic ray acceleration, at least for those particles whose energies do not exceed  $\sim 10^{20}$  eV (for a recent review see Biermann [3]). However, direct observational proof in support of this paradigm has been lacking until recently. The - as some call it - mystery of the source of cosmic rays (CRs) may have been solved with the recent

high-resolution images of TeV emission from supernova remnant SNR RX J1713.7-3946 with HESS (Aharonian et al. [2]). It was the excellent angular correlation between the TeV maps and the X-ray contours from ASCA that proved beyond any reasonable doubt that particle acceleration indeed takes place in the expanding supernova ejecta. The energy spectrum indicates very efficient acceleration of charged particles to energies beyond 100 TeV, as required by the hypothesis that the significant amount of energy stored in form of galactic cosmic rays is due to highly efficient ( $\sim 10\%$ ) accelerators within SNRs.

This observation implies that SNRs should also be luminous continuum sources in the keV - MeV regime. The Compton Observatory mission has detected a significant number of candidate sources (e.g., [28]). Coincidences between EGRET sources and well known SNRs (IC443, W28, W44,  $\gamma$ -Cygni, CTA1) have been reported (e.g., [7]), and emission above 10 keV has been established for SN1006, CTA 1, Cas A, IC443, MSH 11-62, and the remnant discussed in the previous section. While in some of these objects emission from a central pulsar may dominate the high-energy spectrum, in many objects the hard X-ray signature is interpreted as shock acceleration in the remnant, thus supporting the SNR-CR paradigm. The INTEGRAL core program included most of these objects. Preliminary results were published by Sturmer et al. [30].

Flamsteed's remnant Cas A is a well-known calibration source in astronomy (from radio to  $\gamma$ -rays), and perhaps a Rosetta stone for the SNR-CR connection. The presence of electrons with energies of order  $10^{14}$  eV is revealed through their synchrotron continuum emission. The OSSE experiment aboard CGRO determined the hard X-ray spectrum in the 100 keV regime (e.g., [32]) and COMPTEL detected the remnant at 1 MeV Strong et al. [31] and produced upper limits at 10 MeV. EGRET did not detect Cas A above 100 MeV Esposito et al. [10], but HEGRA detected it in the TeV regime [26, 1] INTEGRAL observations of Cas A, essentially a "point source" to IBIS/ISGRI, led to a marginal detec-

tion in the 15-40 keV band and upper limits in the 40-100 keV window [30]. These upper limits are very close to the Cas A spectrum established by previous instruments, and it was thus expected that this  $\sim 300$  year old remnant at  $D \sim 3.4$  kpc would eventually be significantly detected by INTEGRAL. In fact, based on a total of 4.5 Ms exposure time, IBIS/ISGRI has now clearly detected the continuum in the 20-120 keV band, and in addition detected the two lines from the decay of radioactive  $^{44}\text{Ti}$  at 67.9 keV and 78.4 keV [27]. It will take a significantly greater effort to reduce the flux limits on other SNRs for which INTEGRAL observations were reported (CTA 1 and MSH 11-61A), thus making Cas A the key object for a comparison with theory. The key issue is the origin of the emission in the 10-100 keV band, which has been attributed to either synchrotron radiation or non-thermal Bremsstrahlung (e.g., [33]).

Cas A, as well as RX J1713.7-3946 mentioned above, is a member of the growing set of SNRs showing non-thermal X-ray emission. In the latter case, Ellison et al. [8] and Ellison [9] showed that diffusive shock acceleration can produce a broadband continuum spectrum in agreement with the data. One of the key fitting parameters for the models is the strength and geometry of the ambient magnetic field. Here we attempt a self-consistent determination of magnetic field generation and particle acceleration. Ellison et al. [8] also find that the assumed acceleration efficiency (the fraction of the shock energy that is converted to relativistic particles) is of order 50%. Much smaller efficiencies do not lead to successful spectral models and are also inconsistent with the global energy budget required by the SNR-CR connection (e.g., Biermann [3]).

Our microscopic simulations address the question of local requirements in the ejecta needed for such high efficiencies. Vink [33] points out that the presence of a high abundance of cosmic rays may significantly alter the hydrodynamics (as perhaps already observed in 1E 0102.2-7210) and lead to self-regulated CR acceleration as the remnant pressure varies in the transition region between thermally dominated and cosmic ray dominated. X-ray data in the 10-100 KeV regime may hold the key to unraveling the mechanism(s) by which supernovae seed the galaxy with relativistic particles (not limited to electrons). INTEGRAL imaging of the evolved SNR  $\gamma$ -Cygni (Bykov et al. [6]) have revealed highly inhomogeneous flux distributions, suggesting that radiative shocks are present in some fraction of the remnant, but not throughout the system. Non-thermal electron acceleration in evolved remnants interacting in clumpy dense molecular surroundings was studied by Bykov et al. [6], who modeled broad-band emission from SNRs such as  $\gamma$ -Cygni with multi-environments encountered by the shock.

## 2. RPIC SIMULATIONS

Recent PIC simulations using counter-streaming relativistic jets show that acceleration is provided in situ by the two-stream Weibel instability created in the collision-

less shock front, rather than by scattering of particles back and forth across the shock as in Fermi acceleration (Nishikawa et al. [22, 23, 24], Silva et al. [29], Frederiksen et al. [11], Hededal et al. [17], Hededal and Nishikawa [16]). These simulations show that particles are accelerated perpendicular and parallel to the jet's propagation direction and that small-scale highly nonuniform magnetic fields are generated in association with the development of current filaments. The resulting "jitter" radiation from deflected electrons has different properties than standard synchrotron radiation in homogeneous fields Medvedev [18, 19].

In our work a 3-D relativistic particle-in-cell (RPIC) code is used to investigate the spatial development of the collisionless shock front. The evolution of two-stream instabilities is examined in a realistic spatial arrangement, including motion of the contact discontinuity between faster moving and slower moving plasma, e.g., within a jet (internal shocks) or at the jet front (external shock). In our initial investigations, an electron-ion or electron-positron relativistic jet with Lorentz factor  $\gamma = 5$  was injected into an electron-ion Nishikawa et al. [22] or electron-positron plasma Nishikawa et al. [23, 24, 25]. The simulations assume that the jet is injected across the entire inlet plane.

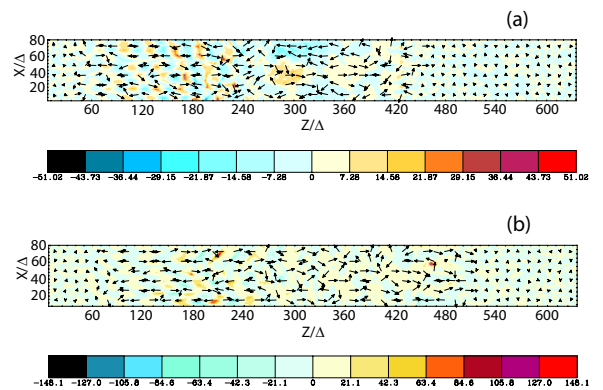


Figure 1. 2D images in the  $x-z$  plane at  $y = 43\Delta$  for the electron-positron jet injected into an unmagnetized ambient electron-positron plasma at  $t = 49.4/\omega_{pe}$ . The colors indicate the  $z$  component of current density generated by the Weibel instability with the  $z$  and  $x$  components of current density represented by arrows for  $\gamma v_{||} = 2$  (a) and 5 (b).

In these 3-D relativistic particle simulations of electron-ion/positron relativistic jets propagating through magnetized and unmagnetized electron-ion/positron ambient plasmas, the Weibel instability is excited in the region behind the jet front and dominates other two-stream instabilities. This predicted result [4, 21] for relativistic collisionless shocks is different than for non-relativistic collisionless shocks where the other two-stream instabilities grow faster than the Weibel instability. The Weibel instability grows as electrons are deflected by growing transverse magnetic fields to enhance a filamented current [34, 20, 4, 12]. The deflection of particle orbits due to the Lorentz force increases as magnetic field perturba-

tions grow in amplitude and the generated magnetic field is randomly oriented in the “shock” plane.

### 3. SIMULATION SETUP

Two simulations are performed using an  $85 \times 85 \times 640$  grid with a total of 380 million particles (27 particles/cell/species for the ambient plasma) and an electron skin depth,  $\lambda_{ce} = c/\omega_{pe} = 9.6\Delta$ , where  $\omega_{pe} = (4\pi e^2 n_e/m_e)^{1/2}$  is the electron plasma frequency and  $\Delta$  is the grid size [24, 25]. In both simulations jets are injected at  $z = 25\Delta$  in the positive  $z$  direction. In all simulations radiating boundary conditions were used on the planes at  $z = z_{\min}, z_{\max}$ . Periodic boundary conditions were used on all other boundaries [5]. The ambient and jet electron-positron plasma has mass ratio  $m_e/m_p \equiv m_{e^-}/m_{e^+} = 1$ . The electron thermal velocity in the ambient plasma is  $v_{th} = 0.1c$  where  $c$  is the speed of light. In this report, electron-positron relativistic jets with Lorentz factor  $\gamma = 2$  ( $v_{jet} = 0.8660c$ ) and 5 ( $v_{jet} = 0.9798c$ ) are injected into an electron-positron ambient plasma.

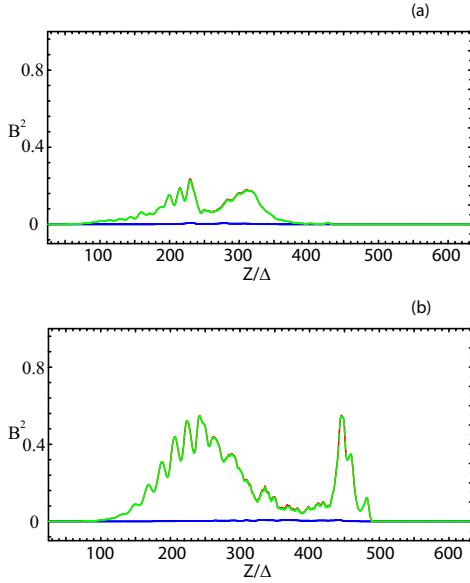


Figure 2. The magnetic field energy density averaged in the  $x - y$  plane along the  $z$ -direction for the electron-positron jet injected into an unmagnetized ambient electron-positron plasma at  $t = 49.4/\omega_{pe}$   $\gamma = 2$  (a) and 5 (b). The total energy density ( $B_x^2 + B_y^2 + B_z^2$ ) is plotted by the red curves, the perpendicular energy density ( $B_x^2 + B_y^2$ ), by green, and the parallel energy density ( $B_z^2$ ), by blue curves.

The perturbed electron density and filamented currents exhibit a complex three-dimensional structure. Figure 1 shows the filamented current ( $J_z$ ). The transverse size is less than the size along the jet direction at the linear stage (not shown). Nonlinear effects lead to merging of the smaller scale filaments that first appear behind the jet

front. The instability is self-saturating behind the jet front and continues until the free energy due to the particle distribution function anisotropy is transferred to the magnetic field.

The slower jet ( $\gamma = 2$ ) shows that the Weibel instability grows earlier as predicted by theory (Medvedev and Loeb 1999) and the current filaments are merged at the nonlinear stage as shown in Fig. 1a. The different nonlinear evolution is shown in the generated current channels in Fig. 1. The jet fronts for both cases are located at  $z/\Delta = 436.4$  and  $490.4$ , respectively. The properties of the synchrotron or “jitter” emission from the “shock” region are determined by the magnetic field strength and structure, and the electron energy distribution [23, 24, 25]. In order to calculate jitter radiation based on simulations of this kind a new method was developed [14, 15]

Figure 2 shows the magnetic field energy for two cases. Since the jet with  $\gamma = 2$  has less kinetic energy, the maximum magnetic field energy is also small. The slower jet has small magnetic field near the jet head. On the contrary, the faster jet shows an isolated strong magnetic field at the jet head.

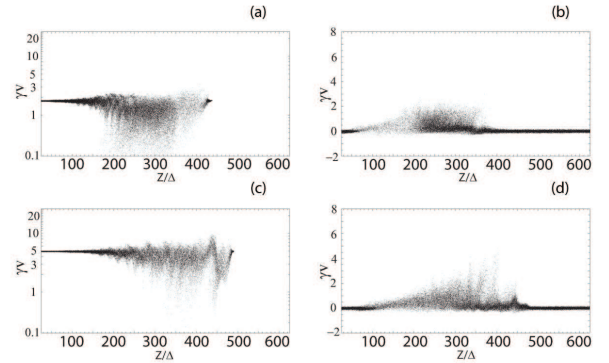


Figure 3. Distributions of jet (left column) and ambient (right column) electrons in  $Z/\Delta - \gamma V_{\parallel}$  phase spaces for  $\gamma = 2$  (a and b) and 5 (c and d) at  $t = 49.4/\omega_{pe}$ . Jet electrons ( $25 < Z/\Delta < 625$ ) are randomly selected for these plots.

Figure 3 shows the phase-space distributions ( $Z/\Delta - \gamma V_{\parallel}$ ) of jet and ambient electrons for both cases at  $t = 49.4/\omega_{pe}$ . The left column (a and c) shows phase-space distributions for electrons with  $\gamma = 2$  and 5, respectively. The basic structures are similar. The jet heads are separated from the main jets. As shown in Fig. 2, the jet head with slower jet has weak magnetic field ( $350 < z/\Delta < 430$ ). The strong magnetic field is consistent with the jet head ( $440 < z/\Delta < 480$ ). The ambient electrons are efficiently accelerated with the slow velocity as shown in Fig. 3b. Furthermore, the ambient electrons are strongly accelerated and dragged by the jet, therefore the ambient electron density becomes smaller in the linear region ( $100 < z/\Delta < 180$ ). The ambient electrons with the fast jet are accelerated up to the initial jet velocity in the nonlinear region.

#### 4. SUMMARY AND DISCUSSIONS

The initial work makes it clear that the composition of the plasma [23] and/or the Alfvén speed can make a significant difference in the dominant instabilities [16], in the generated magnetic field and in the acceleration of particles in the relativistic collisionless shock. We anticipate that the orientation of the magnetic field, the value of the Lorentz factor, and the plasma temperature will all play a significant role in the processes occurring within relativistic collisionless shocks. For example, the growth rate of various two-stream instabilities is affected by the Lorentz factor [4, 23], by different strength of the ambient (unperturbed) magnetic field [13], and by thermal motion of the ambient plasma [35, 20].

The structures of jets with two different velocities are substantially different. This is due to the fact that other two-stream instabilities occur besides the Weibel instability [21]. One of the specific differences is the structure of the jet head. The jet head in relativistic jets ( $\gamma > 5$ ) has a distinctive jet front, separated from the rest of jet with locally strong magnetic fields. In contrast, the slower jet has a jet front without a localized magnetic field.

The observed flow velocities are not relativistic in SNRs. In general observed multi-layer structures are consistent with simulation results of clumped density within a slow jet, which slows down due to the interaction with the surrounding medium.

#### ACKNOWLEDGMENTS

K. N. is partially supported by the National Science Foundation awards ATM-0100997, INT-9981508, and AST-0506719, and the National Aeronautic and Space Administration award NNG05GK73G to the Univ of Alabama in Huntsville. P.H. acknowledges partial support by a National Space Science and Technology (NSSTC/NASA) cooperative agreement NCC8-256 and NSF awards AST-0506666. Y. M. is a NASA Postdoctoral Program fellow at NASA Marshall Space Flight Center. The simulations have been performed on IBM p690 at the National Center for Supercomputing Applications (NCSA) which is supported by the NSF.

#### REFERENCES

[1] Aharonian, F. A. et al. 2001, *A&A* 370, 112  
[2] Aharonian, F. A. et al. 2004, *Nature* 432, 75  
[3] Biermann, P. 2003, *New Astron. Rev.* 48, 41  
[4] Brainerd, J.J. 2000, *ApJ* 536, 628  
[5] Buneman, O., 1993, *Tristan*, in *Computer Space Plasma Physics: Simulation Techniques and Software*, edited by H. Matsumoto Matsumoto & Y. Omura, p. 67, Terra Scientific Publishing Company, Tokyo

[6] Bykov, A. M., et al. 2004, *A&A* 427, L21  
[7] Cheng, K. S. and Romero, G. (eds) 2004, *Astrophys. Space Sci. Lib* (Kluwer)  
[8] Ellison, D. C., Slane, P., and Gaensler, B. M. 2001, *ApJ* 563, 191  
[9] Ellison, D. C. 2002, *New Astron. Rev.* 46, 503  
[10] Esposito, J. A. et al. 1996, *ApJ* 461, 820  
[11] Frederiksen, J. T., Hededal, C. B., Haugbølle, & Nordlund, Å. 2004, *ApJ* 608, L13.  
[12] Gruzinov, A. 2001, *ApJ* 563, L15  
[13] Hardee, P.E. 1978, *ApJ* 219, 274  
[14] Hededal, C.B. 2005 Ph.D. thesis (astro-ph/0506559)  
[15] Hededal, C.B., Nordlund, Å. 2005, submitted to *ApJL* (astro-ph/0511662)  
[16] Hededal, C.B., Nishikawa, K.-I. 2005, *ApJ* 617, L107  
[17] Hededal, C.B., Frederiksen, J. T., Haugbølle, T. Nordlund, Å. 2004, *ApJ*, 617, L107  
[18] Medvedev, M. V. 2000, *ApJ* 540, 704  
[19] Medvedev, M. V. 2006, *ApJ* 637, 869  
[20] Medvedev, M.V., & Loeb, A. 1999, *ApJ* 526, 697  
[21] Medvedev, M. V., Silva, L. O. Kamionkowski, M. 2006, *ApJL* 642, L1  
[22] Nishikawa, K.-I., Hardee, P., Richardson, G., Preece, R., Sol, H., & Fishman, G.J. 2003 *ApJ* 595, 555  
[23] Nishikawa, K.-I.; Hardee, P.; Richardson, G.; Preece, R.; Sol, H.; Fishman, G. J. 2005, *ApJ* 623, 927  
[24] Nishikawa, K.-I., Hardee, P., Hededal, C. B., Fishman, G. J. 2006a, *ApJ* 642, 1267  
[25] Nishikawa, K.-I., Hededal, C. B., Hardee, P., Fishman, G. J., Kouveliotou, C., Mizuno, Y. 2006b, *Astrophys Space Sci*, DOI 10.1007/s10509-006-9234-5  
[26] Pühlhofer, G., et al. 1996, *Proc. 26th ICRC*, 3, 492  
[27] Renaud, M., Vink, J. et al. 2006, *ApJ* 647, L41  
[28] Schönfelder, V. et al. 2001, (ed) "The Universe in Gamma Rays" (Springer)  
[29] Silva, L. O., Fonseca, R. A., Tonge, J., W., Dawson, J. M., Mori, W.B., Medvedev, M. V. 2003, *ApJ* 596, L121  
[30] Sturmer, S. J., et al. 2004, *Proc. 5th INTEGRAL Science Workshop*, ESA SP-552, p. 497  
[31] Strong, A., et al. 2000, *Proc. 5th Compton Symposium*, AIPC 510, p. 60  
[32] The, L.-S. et al. 1997, *Proc. 4th Compton Symposium*, AIPC 410, p. 1147  
[33] Vink, J. 2004, *AdSpR* 33, 356  
[34] Weibel, E. S. 1959, *Phys. Rev. Lett.* 2, 83  
[35] Yoon, P.H. & Davidson, R.C. 1987, *Phys.Rev.A*, 35, 2718